Hindawi
Advances in Civil Engineering
Volume 2022, Article ID 2209394, 9 pages
https://doi.org/10.1155/2022/2209394

Research Article

Numerical Researches of Rectangular Barge in Variable Bathymetry Based on Boussinesq-Step Method

Yan Su

School of Ocean Engineering and Technology, Sun Yat-sen University, Guangzhou, China

Correspondence should be addressed to Yan Su; suyan23@mail.sysu.edu.cn

Received 17 March 2022; Accepted 4 July 2022; Published 18 August 2022

Academic Editor: Cristoforo Demartino

Wave responses of the rectangular barge in variable bathymetry are investigated by combining the Boussinesq-type equations and the step method. The highly accurate Boussinesq-type equations in terms of velocity potential are adopted for simulating the evolution of waves along the inclined beach. Hydrodynamic coefficients of a rectangular barge floating on the inclined bottom are calculated by the step method in the frequency domain. Based on the impulse response function method, the motions of the barge can be predicted in the time domain. The Haskind relation is used to reform the wave exciting forces, and the mean offset in the sway motion is also given based on the mean drift force. The wave responses of the barge at different locations along the inclined beach are measured in the experiments. Compared with experimental results, the solutions of the Boussinesq-step method present an overall good agreement.

1. Introduction

Predicting wave responses of a floating body in restricted water depth has been the subject of extensive effects over the years. With the development of LNG (liquefied natural gas) consumption, projects of LNG offloading terminals and LNG floating storage units are continually carried out. Offloading terminals or FSRUs (floating storage regasification units) would be located in exposed shallow water area.

The major challenges of predicting wave responses of a floating body in variable bathymetry are the nonlinearities of wave propagation in the coastal zone and the wave-structure interactions considering the effects of the seabed. A variety of numerical models have been developed to solve the complex problem. With the increase of computational powers, various computational fluid dynamic (CFD) models have been applied, such as models based on Reynolds-averaged Navier-Stokes (RANS) equations (Stern et al. [1]; Rijnsdorp and Zijlema [2]) and models based on smoothed particle hydrodynamics (SPH) methods (Bouscasse et al. [3]; Ren et al. [4]). However, computational limitations restrict the application of such highly detailed models to relatively small scales, spanning only a few wavelengths and wave periods.

Potential flow theory has also been a popular approach to solve the wave-structure interactions. Both the boundary element method (BEM) (Belibassakis [5]; You and Faltinsen [6]; Xiong et al. [7]) and the finite element method (FEM) (Yan and Ma [8]; Ma and Yan [9]) have been developed to simulate wave responses of a floating body in offshore and coastal regions.

Coupled approaches including wave propagation models and wave-ship interaction models have been built (Bingham [10]; Pinkster and Naaijen [11]; Wim van der and Ivo [12]; Dobrochinski [13]). Following Bingham [10], the Boussinesq-type equations in terms of velocity were used to predict the transformation of waves from the deep water into the harbour where the ship was moored. Linear wave radiation and diffraction forces were computed using a constant-strength panel method in the frequency domain. The equation of motions in the time domain was used for simulating the motions of a moored ship. Different from Bingham [10], a time-domain panel method was applied to determine the scattering of incident waves in Wim Van der and Ivo [12].

In this paper, wave responses of a rectangular barge moored at different positions along an inclined beach are

studied based on the hybrid Boussinesq-step method. Wave propagation along the inclined beach is simulated by highly accurate Boussinesq-type equations in terms of velocity potential which is proposed in Bingham et al. [14]. Hydrodynamic coefficients of the barge in variable bathymetry are obtained based on the step method where the effects of the seabed can be considered. The motions of the barge in waves are calculated by the impulse response function approach. Here, the wave exciting forces are reformed by the Haskind relations which include the incident wave quantities and solutions to the radiation problem. The mean offsets of sway motions are given based on the mean drift force. The solutions of the Boussinesq-step method present an overall good agreement with the experimental results.

2. Numerical Methods

2.1. Boussinesq-Type Equations. The potential theory which assumed inviscid, irrotational, and incompressible flow is adopted. A Cartesian coordinate system is adopted here, with the origin located on the still water plane and the z-axis pointing vertically upwards. The boundaries of the fluid domain are given by the bottom at $z = -h(\mathbf{x})$ and the free surface at $z = \eta(\mathbf{x}, t)$ with $\mathbf{x} = [x, y]$. Following Zakharov [15], the following free surface boundary conditions are written in terms of the velocity potential $\widetilde{\Phi} = \Phi(\mathbf{x}, \eta, t)$ and the vertical velocity $\widetilde{w} = (\Phi_z)_{z=\eta}$ defined directly on the free surface:

$$\begin{aligned} \eta_t + \nabla\eta \cdot \nabla\widetilde{\Phi} - \widetilde{w}(1 + \nabla\eta \cdot \nabla\eta) = 0, \\ \widetilde{\Phi}_t + g\eta + \frac{1}{2}(\nabla\widetilde{\Phi})^2 - \frac{1}{2}\widetilde{w}^2(1 + \nabla\eta \cdot \nabla\eta) = 0, \end{aligned} \tag{1}$$

where $\nabla = [\partial/\partial x, \partial/\partial y]$ is the horizontal gradient operator, and g is the gravitational acceleration.

The Laplace equation in the fluid domain and the kinematic boundary condition on the bottom are given as follows:

$$\begin{aligned} \nabla^2\Phi + \Phi_{zz} = 0, \\ w + \nabla h \cdot \nabla\Phi = 0, \\ z = -h(\mathbf{x}). \end{aligned} \tag{2}$$

Following Bingham et al. [14], Taylor series expansion of the solution $\Phi(\mathbf{x}, z, t)$ about an arbitrary vertical position $z = \hat{z}(\mathbf{x})$ is given by

$$\Phi(\mathbf{x}, z, t) = \hat{\Phi} + (z - \hat{z}(\mathbf{x}))\hat{w} + \frac{1}{2}(z - \hat{z}(\mathbf{x}))^2\hat{\Phi}^{(2)} + \cdots, \tag{3}$$

where

$$\begin{aligned} \hat{\Phi} = \hat{\Phi}^{(0)} = \Phi(\mathbf{x}, \hat{z}(\mathbf{x}), t), \\ \hat{w} = \hat{\Phi}^{(1)} = \frac{\partial\Phi(\mathbf{x}, \hat{z}(\mathbf{x}), t)}{\partial z}, \\ \hat{\Phi}^{(n)} = \left.\frac{\partial^n\Phi(\mathbf{x}, z, t)}{\partial z^n}\right|_{z=\hat{z}(\mathbf{x})}, \quad n = 2, 3, \cdots, \infty. \end{aligned} \tag{4}$$

Substituted into the Laplace equation, a recursion relation of different order vertical derivatives of velocity potential $\hat{\Phi}^{(n)}$ can be obtained.

$$\hat{\Phi}^{(n)} = \frac{-\nabla^2\hat{\Phi}^{(n-2)} + 2\nabla\hat{z} \cdot \nabla\hat{\Phi}^{(n-1)} + \nabla^2\hat{z} \cdot \hat{\Phi}^{(n-1)}}{1 + \nabla\hat{z}^2}. \tag{5}$$

The recursion relation can be simplified based on assuming a small bottom slope that is $\hat{z}(\delta\mathbf{x})$ where $\delta \ll 1$. Collecting terms at each order of δ and keeping terms up to δ, we get

$$\hat{\Phi}^{(n)} = -\nabla^2\hat{\Phi}^{(n-2)} + 2\delta\nabla\hat{z} \cdot \nabla\hat{\Phi}^{(n-1)}. \tag{6}$$

Successively solving for $n = 2, 3, \cdots, \infty$, Φ can be expressed in terms of $\hat{\Phi}$ and $\hat{w}$. In order to improve the accuracy of the truncated approximation, an enhancement operator with new expansion variables $\hat{\Phi}^*$, $\hat{w}^*$ is adopted.

$$\hat{\Phi} = L_p(\hat{z}\nabla)\hat{\Phi}^*, \hat{w} = L_w(\hat{z}\nabla)\hat{w}^*. \tag{7}$$

Finally, the Taylor series expansion of velocity potential can be reformed and expressed in terms of velocity potential and vertical velocity defined on an arbitrary vertical position.

$$\Phi(\mathbf{x}, z, t) = \left(J_{01} + \delta\nabla\hat{z} \cdot J_{11p}\nabla\right)\hat{\Phi}^* + \left(J_{02} + \delta\nabla\hat{z} \cdot J_{12p}\nabla\right)\hat{w}^*. \tag{8}$$

The same procedure can be applied to the horizontal and vertical velocities

$$\begin{aligned} \mathbf{u}(\mathbf{x}, z, t) = \left(J_{01}\nabla + \delta\nabla\hat{z}J_{11u}\right)\hat{\Phi}^* + \left(J_{02}\nabla + \delta\nabla\hat{z}J_{12u}\right)\hat{w}^*. \\ w(\mathbf{x}, z, t) = \left(-J_{02}\nabla^2 - \delta\nabla\hat{z} \cdot J_{12w}\nabla\right)\hat{\Phi}^* \\ + \left(J_{01} + \delta\nabla\hat{z} \cdot J_{11w}\nabla\right)\hat{w}^*. \end{aligned} \tag{9}$$

Here, $\hat{\Phi}^*$ and $\hat{w}^*$ are unknown variables, and J_{01}, J_{02}, J_{11p}, J_{12p}, J_{11w}, J_{12w}, J_{11u}, J_{12u} are known operators defined by Bingham et al. [14].

The numerical solution of the above-described Boussinesq-type model has been implemented based on the finite difference method. The details of the method can be found in Jamois [16]. A structured grid of N_x by N_y points is distributed over the rectangular still water plane. Homogeneous Neumann boundary conditions at the side walls of the domain are imposed by reflecting the finite difference coefficients for a function that is symmetric about the boundary, and thus, all schemes are effectively centred. Free surface boundary conditions are evolved forward from initial conditions using the classical explicit fourth-order Runge–Kutta scheme (Quarteroni et al. [17]). This linear system of equations is solved using GMRES iterative scheme (Saad and Schultz [18]) preconditioned by an incomplete LU factorisation.

2.2. Step Method. In the framework of potential flow theory, the hydrodynamic coefficients of the barge with the inclined bottom are solved by the step method in the frequency domain. The variable bathymetry region is decomposed as a

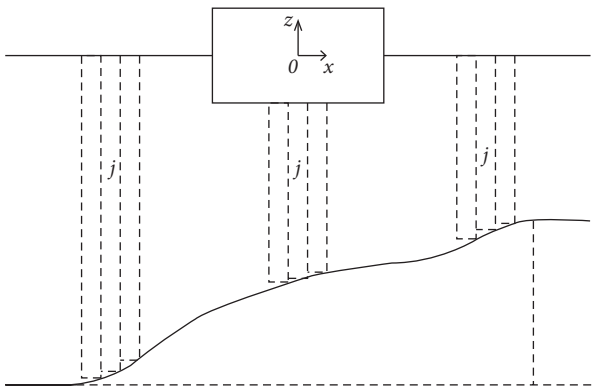

Figure 1: Sketch of a succession of rectangular subdomains.

series of horizontal steps and defined as a succession of rectangular subdomains in Figure 1.

Eigen-function expressions are used to express the velocity potential in each subdomain. For the first-order diffraction problem, the velocity potential in each subdomain j on the left and right sides of barge can be written as follows (Liu et al. [19]):

$$\phi_j(x,z) = \frac{\cosh k_{j0}\left(z+h_j\right)}{\cosh k_{j0}h_j}\left[B_{j0}e^{ik_{j0}\left(x-x_l\right)} + C_{j0}e^{-ik_{j0}\left(x-x_r\right)}\right] + \sum_{m=1}^{\infty}\cos k_{jm}\left(z+h_j\right) \cdot \left[B_{jm}e^{-k_{jm}\left(x-x_l\right)} + C_{jm}e^{k_{jm}\left(x-x_r\right)}\right]. \tag{10}$$

Also, for the subdomains j below the barge, the velocity potential can be written as follows:

$$\phi_j(x,z) = B_{j0} + C_{j0}\frac{x}{L}, + \sum_{m=1}^{\infty}\cos\lambda_{jm}\left(z+h_j\right) \cdot \left[B_{jm}e^{-k_{jm}\left(x-x_l\right)} + C_{jm}e^{k_{jm}\left(x-x_r\right)}\right]. \tag{11}$$

The wave numbers k_{jm} and λ_{jm} satisfy the following equations:

$$\omega^2 = gk_{j0}\tanh k_{j0}h_j = -gk_{jm}\tan k_{jm}h_j, \qquad \lambda_{jm} = \frac{m\pi}{h_j - d}. \tag{12}$$

Here, L is the length and d is the draft of the barge. x_l and x_r are the left and right horizontal coordinates of each subdomain, respectively. h_j is the depth of each subdomain. ω is the circular frequency of the incident wave. B_{jm} and C_{jm} are unknown coefficients that can be solved based on the continuity of velocity potential and horizontal velocity along the connected lines:

$$\phi_j = \phi_{j+1} \quad \frac{\partial\phi_j}{\partial x} = \frac{\partial\phi_{j+1}}{\partial x}. \tag{13}$$

The radiation potential φ_j can be given by adding up a particular solution to the results obtained from the fixed barge. For the heave and roll motions, the particular solutions are expressed as follows:

$$\frac{\left(z+h_j\right)^2 - x^2}{2\left(h_j - d\right)} \quad \frac{\left(x-x_g\right)}{2\left(h_j-d\right)}\left\{\frac{\left(x-x_g\right)^2}{3} - \left(z+h_j\right)^2\right\}, \tag{14}$$

where x_g is the horizontal coordinate of the center of gravity. Moreover, hydrodynamic coefficients are calculated by integrating radiation potential along the wetted surfaces of barge.

For the irregular wave, a superposition of first-order wave components with different amplitudes and frequencies can be adopted. The second-order approximation produces the wave loads oscillating with the sum and difference frequencies. Therefore, second-order loads, even though much smaller than first-order ones, cover a much wider range of frequencies. Difference frequency second-order loads are responsible for much behavior as the slow drift motion of moored structures (Molin [20]). Here, the mean offsets of the barge are considered based on the mean drift force in irregular waves computed by Liu et al. [19].

$$F_d = 2\int_0^{\infty} S(\omega) f_d(\omega) d\omega. \tag{15}$$

$S(\omega)$ is the incident wave spectral density calculated by the numerical wave tank based on the Boussinesq-type equations, and $f_d(\omega)$ is the normalized drift forces by amplitudes squared in regular waves obtained from the step method. Two well-known formulations of wave drift force are as follows: the far-field method based on momentum considerations introduced by Maruo [21] and extended by Newman [22]; the near-field method based on direct pressure integration proposed by Pinkster and Van Oortmerssen [23]. For the variable bathymetry, the control contour in the far-field method consists of two vertical cuts away from the barge and the sea floor in-between. But the rectangular contour in-between the barge and varying bottom exhibit poor numerical convergence (Liu [24]). So the near-field method is adopted here for the values of drift force (Pinkster and Van Oortmerssen [23]).

2.3. Equations of Motions. The general equations of motions in the time domain can be written as follows ($i = 1, \ldots, 6$):

$$\sum_{j=1}^{6}\left\{\left(M_{ij} + m_{ij}\right)\ddot{x}_j + \int_{-\infty}^{t} K_{ij}(t-\tau)\dot{x}_j(\tau)d\tau + C_{ij}x_j\right\} = F_i. \tag{16}$$

Here, M_{ij} is the inertia matrix, and m_{ij} is the infinite frequency added mass matrix. K_{ij} is the retardation function, and C_{ij} is the matrix of hydrostatic restoring stiffness.

x_j is the motions of the floating body. F_i is the time-varying exciting forces (Cummins [25]).

A quadratic damping term, nonlinear viscous roll damping contributions, is added on the right side of the roll equation of motion:

$$C_{v4} = -\frac{1}{2}\rho C_d B^4 L|\dot{\alpha}|\dot{\alpha}, \tag{17}$$

where C_d is drag coefficient and equal to 0.2. B is the beam of barge, and L is the length. $\dot{\alpha}$ is the roll velocity. The quadratic viscous damping for drift motion is given by

$$-\frac{1}{2}\rho C_d L d|\dot{Y}|\dot{Y}. \tag{18}$$

The drag coefficient was taken from still water decay tests, which gave $C_d = 5$ at 54 cm depth, $C_d = 6$ at 29 cm depth, and $C_d = 7$ at 21 cm depth. $\dot{Y}$ is the sway velocity.

The retardation functions and the frequency-independent added masses are related to the added masses and damping coefficients which can be calculated by the step method in the frequency domain.

$$K_{ij}(\tau) = \frac{2}{\pi}\int_0^\infty b_{ij}(\omega)\cos(\omega\tau)d\omega,$$
$$m_{ij} = a_{ij}(\Omega) + \frac{1}{\Omega}\int_0^\infty K_{ij}(t)\sin(\Omega t)dt, \tag{19}$$

where Ω is an arbitrarily chosen value of the frequencies. a_{ij} and b_{ij} are the added masses and damping coefficients, respectively.

The wave exciting forces F_i can be expressed in various ways, but it is convenient here to employ the Haskind relations and write it in terms of incident wave quantities and solutions to the radiation problem. The time-varying wave exciting force can be calculated by the inverse Fourier transforms.

$$F_i(t) = \frac{1}{2\pi}\int_{-\infty}^{\infty} F_i(\omega)e^{i\omega t}d\omega. \tag{20}$$

Also, the exciting force in the frequency domain can be expressed as follows:

$$F_i(\omega) = \iint_{S_b} d\vec{x}\,P(\vec{x},\omega)n_i(\vec{x}),$$
$$+ i\omega\rho\iint_{S_b} d\vec{x}\,\varphi_i(\vec{x},\omega)\Phi_n(\vec{x},\omega). \tag{21}$$

Φ is the incident wave velocity potential. A subscript n is used to indicate the operation $\mathbf{n}\cdot\nabla$, with $\mathbf{n}$ is the normal vector to the equilibrium wetted body surface S_b. The dynamic pressure P and the velocity $\nabla\Phi$ on the free surface can be given based on the solutions of Boussinesq-type equations. φ_i is the solution to the ith-mode impulsive velocity radiation problem solved by the step method. n_i is the generalized normal vector.

3. Wave Responses of Barge

3.1. Experimental Setup. Experiments were carried out in the BGO-first offshore tank located in La Seyne-sur-Mer, and the preliminary researches of experimental data were given by Liu et al. [19]. The basin has a total length of over 40 meters and a width of 16 meters. In the experiments, the false bottom was raised and inclined at a slope of 5%, starting from a depth of 1.05 m by the wavemaker side, and emerging by 15 cm at its other end (Figure 2).

Figure 2: Barge in the basin.

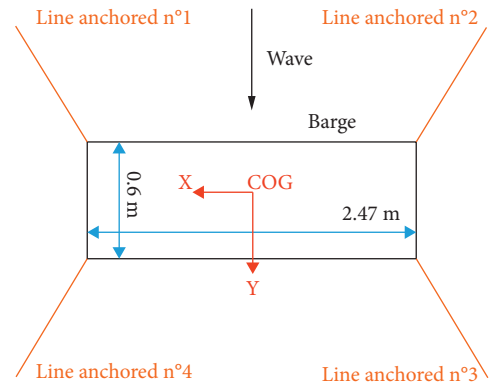

Figure 3: Aerial lines connected to the barge in the basin (top view).

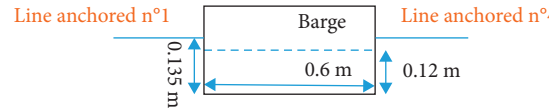

Figure 4: Aerial lines connected to the barge in the basin (side view).

The rectangular barge model has a length of 2.47 m, a beam of 0.6 m, and a draft of 0.12 m. The coordinate system and the dimensions of barge have been marked in Figure 2. The center of gravity (CoG) is located at 0.135 m above the keel line, and the roll radius of gyration is equal to 0.19 m. Four aerial lines connected to the barge corners at the CoG level and terminated at the basin walls. The top view and side view of experimental settings are shown in Figures 3 and 4. Each line was constituted by a steel cable of 1 mm in diameter and terminated by springs. The stiffness of each line numbered from 1 to 4 was 72.7 N/m, 73.7 N/m, 72.9 N/m,

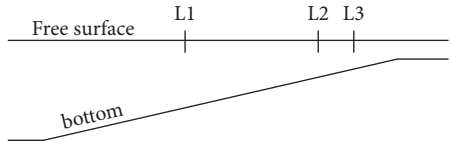

Figure 5: Locations of barge in the basin.

and 72.1 N/m, respectively. The global sway stiffness was 150 N/m yielding the sway natural period of around 10 seconds.

The irregular waves of Pierson–Moskowitz spectra with the peak period (T_p) of 1.2 seconds were selected and the significant wave heights (H_s) were equal to 2, 4, and 6 cm respectively. Test duration in the irregular waves was 1200 s. The water depths of different barge locations were 54 cm ($L1$), 29 cm ($L2$), and 21 cm ($L3$) (Figure 5).The motions of barge were measured by the optical system KRYPTON RODYM CMM. The system is a camera-based measurement system that triangulates the position of the target for contactless measurement and evaluation of six degrees of freedom motions.

3.2. Numerical Results. The wave responses of barge in variable bathymetry can be calculated based on the equations of motions in the time domain. Hydrodynamic coefficients are obtained from the step method where the variable bathymetry can be considered. It is important to stress that the incident wave is a long-crested beam wave and the wavemaker line is parallel to the longitudinal axis of barge and the inclined bottom plane. The bottom is not oriented arbitrarily. Only the sway, heave, and roll barge motions in the vertical plane are considered. So the hydrodynamic coefficients of barge are reasonably simplified as two-dimensional results of the step method multiplied by the length of the barge. The fluid domain is divided into 100 rectangular subdomains and the range of computational frequencies is set from 0.2 rad/s to 20.0 rad/s with the interval of 0.2 rad/s. The Haskind relation is used to reform the wave exciting force in terms of incident wave quantities given by the Boussinesq-type equations.

The time histories of sway, heave, and roll motions of barge calculated by the numerical model are shown in Figures 6–8. The significant waveheight is 0.06 m, and the peak period is 1.2 second. The water depth of barge location is 21 cm.

As shown in Figures 9–11, the spectral densities of sway motions at different locations ($L1$, $L2$, and $L3$) are shown under different incident waves. With the augment of significant waveheights, the peak values of spectral densities of sway motions become higher. Meanwhile, the spectral densities at locations ($L2$ and $L3$) are obviously higher than at the location $L1$ under the same incident wave conditions. The coupled sway and roll motions can be found in both the numerical and experimental results, which lead to the second peak around 6 rad/s. The significant discrepancy between the numerical results and the experimental data can be found at the location $L1$. The discrepancy is due to the viscous damping of coupled motions which should be studied further.

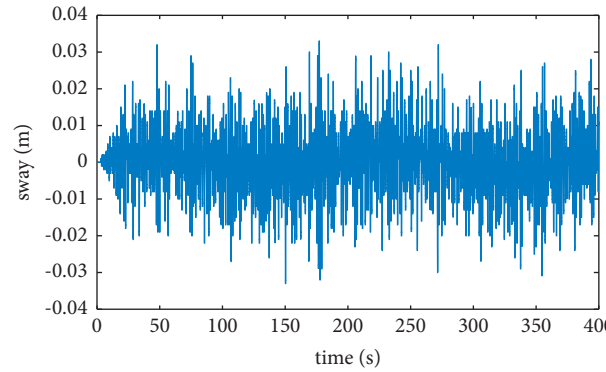

Figure 6: The time histories of sway motions at $L3$. $T_p = 1.2$ s, $H_s = 0.06$ m.

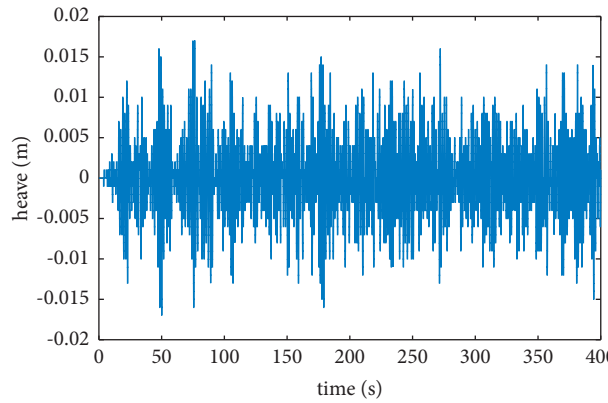

Figure 7: The time histories of heave motions at $L3$. $T_p = 1.2$ s, $H_s = 0.06$ m.

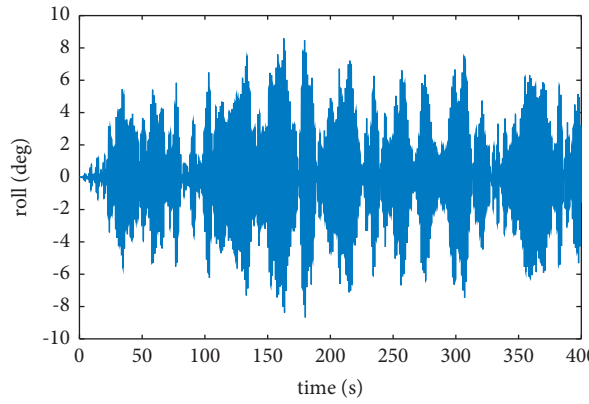

Figure 8: The time histories of roll motions at $L3$. $T_p = 1.2$ s, $H_s = 0.06$ m.

For the heave motions in Figure 12, smaller peak values of spectral densities can be found with the lower water depth due to the effects of the bottom. At location $L3$, the spectral densities of numerical results and experimental data are different (Figure 12(c)). For the shallow-water conditions,

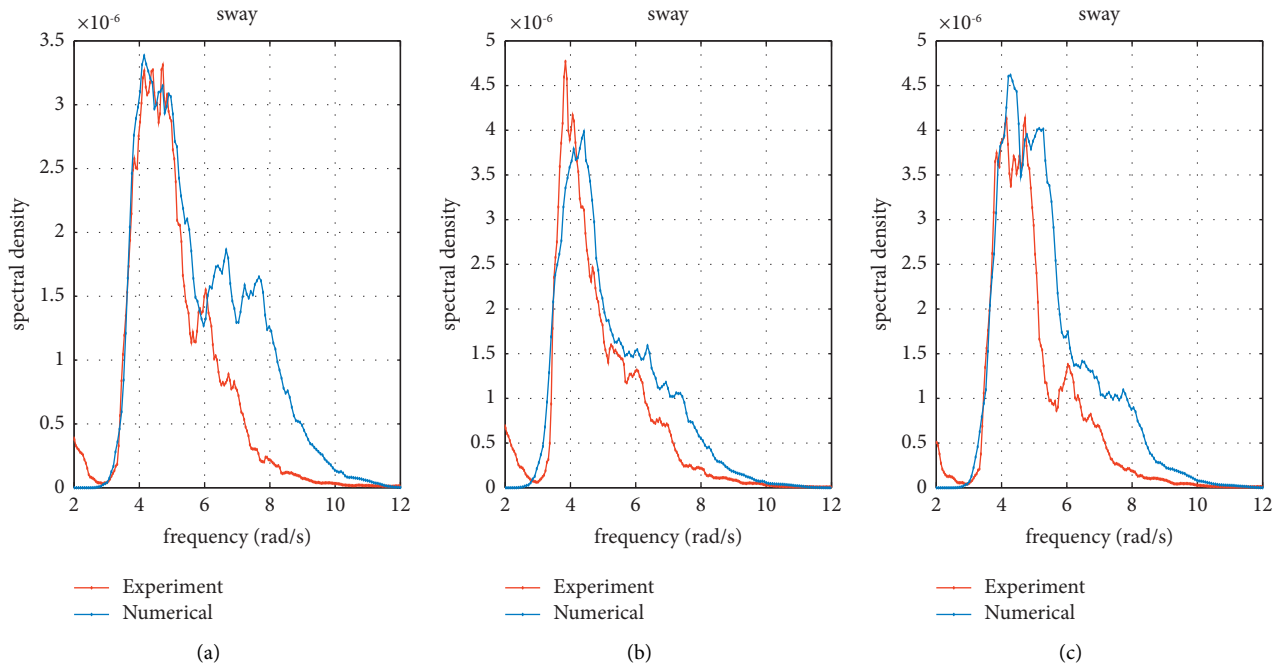

Figure 9: Comparisons of spectral densities of sway motions: $T_p = 1.2$ s, $H_s = 0.02$ m, $L1$ (a), $L2$ (b), $L3$ (c).

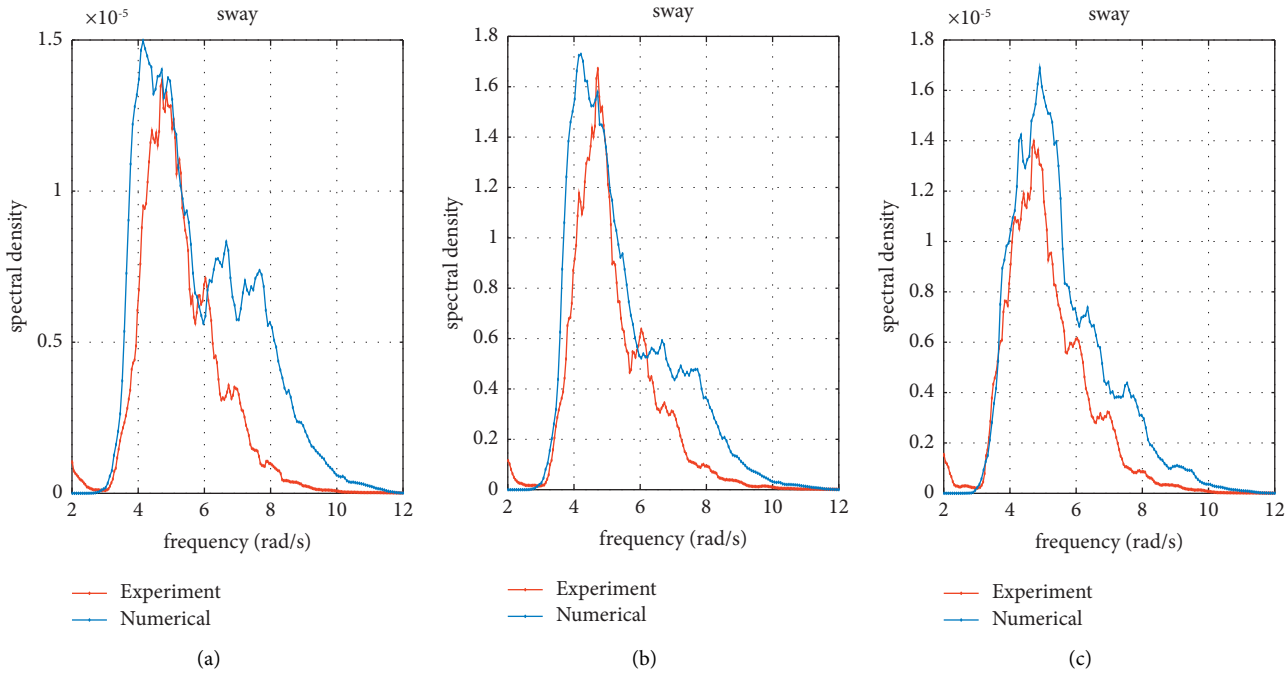

Figure 10: Comparisons of spectral densities of sway motions: $T_p = 1.2$ s, $H_s = 0.04$ m, $L1$ (a), $L2$ (b), $L3$ (c).

the nonlinear interaction between shallow-water waves and barge should be studied further.

The spectral densities of roll motions are compared in Figure 13 with the peak period of incident waves 1.2 second and the significant wave height of incident waves 0.02 meter. The numerical results of spectral densities are a little lower than the experimental data at different barge locations ($L1$, $L2$, and $L3$). The quadratic damping term for considering the viscous roll damping contributions is not very applicable for shallow-water conditions.

The mean drift force of the barge in irregular waves is calculated by equation (19). The spectral density of the incident wave is obtained from the Boussinesq-type equations, and normalized drift force is given by the step

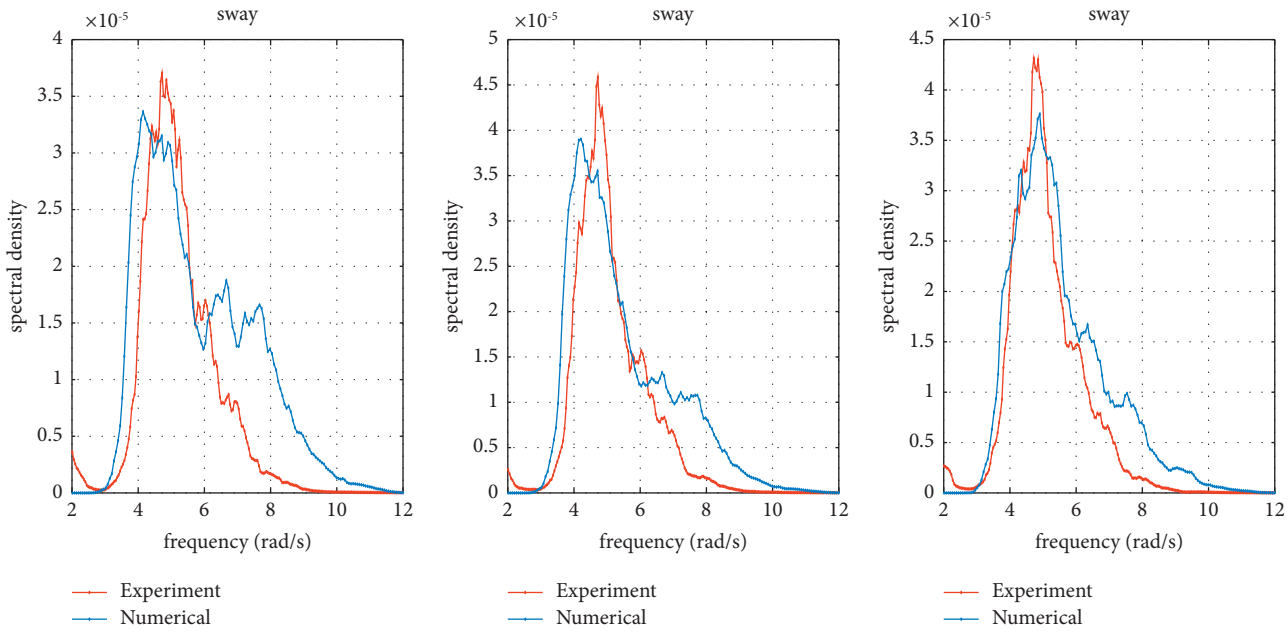

Figure 11: Comparisons of spectral densities of sway motions: $T_p = 1.2$ s, $H_s = 0.06$ m, $L1$ (a), $L2$ (b), $L3$ (c).

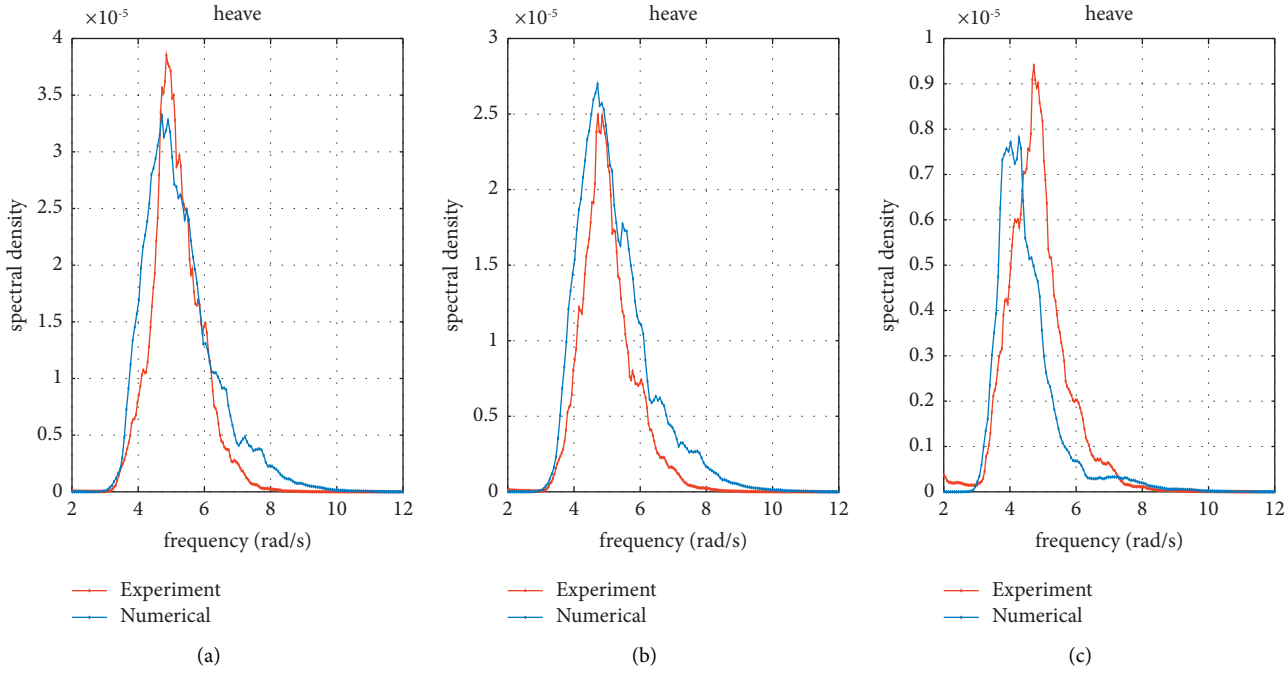

Figure 12: Comparisons of spectral densities of heave motions: $T_p = 1.2$ s, $H_s = 0.04$ m, $L1$ (a), $L2$ (b), $L3$ (c).

method and near-field equation. The mean offset is equal to the mean drift force divided by the 150 N/m stiffness. The following tables (Tables 1–3) show the calculated and measured mean offsets (normalized by the significant wave height squared) for different sea states and initial locations of barge. Viewing from the comparisons in the tables, the numerical model can predict well the mean offsets of sway motions.

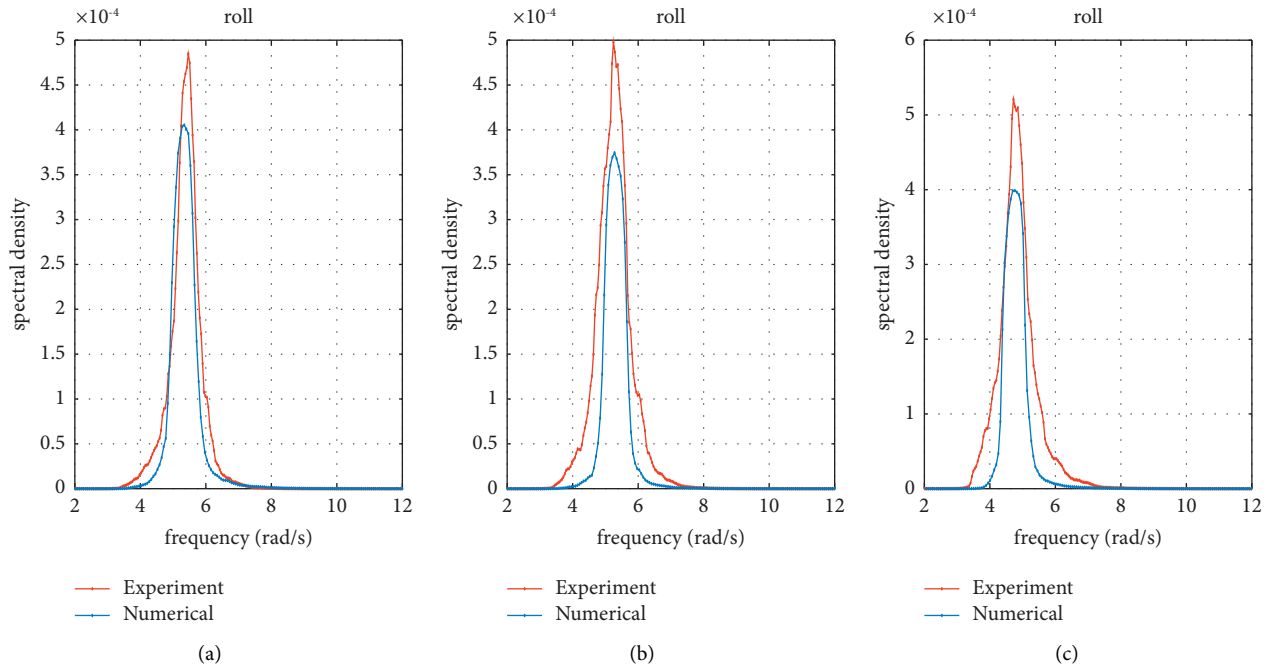

Figure 13: Comparisons of spectral densities of roll motions: $T_p = 1.2$ s, $H_s = 0.02$ m, $L1$ (a), $L2$ (b), $L3$ (c).

Table 1: Mean offsets in $T_p = 1.2$ s, $H_s = 2.0$ cm.

$T_p = 1.2$ s, $H_s = 2.0$ cm	$L1$	$L2$	$L3$
Measured (m^{-1})	8.6	9.8	13.5
Calculated (m^{-1})	7.9	9.1	11.2

Table 2: Mean offsets in $T_p = 1.2$ s, $H_s = 4.0$ cm.

$T_p = 1.2$ s, $H_s = 4.0$ cm	$L1$	$L2$	$L3$
Measured (m^{-1})	8.5	9.7	12.7
Calculated (m^{-1})	7.8	9.0	11.2

Table 3: Mean offsets in $T_p = 1.2$ s, $H_s = 6.0$ cm.

$T_p = 1.2$ s, $H_s = 6.0$ cm	$L1$	$L2$	$L3$
Measured (m^{-1})	8.4	9.5	11.8
Calculated (m^{-1})	7.8	8.9	11.1

4. Concluding Remarks

The hybrid Boussinesq-step method was constructed to predict wave responses of a rectangular barge moored at different positions along the inclined beach. Highly accurate Boussinesq-type equations in terms of velocity potential were used for simulating the propagation of waves. Hydrodynamic coefficients of barge with inclined bottom were calculated by the step method in the frequency domain. The motions of the barge in the irregular waves were computed based on the impulse response function approach, and the wave exciting forces were reformed by the Haskind relations.

The hybrid Boussinesq-step method accounts for the most important physical processes involved in the floating body in restricted water while keeping the computational burden modest. The spectral densities of sway, heave, and roll motions of barge with different water depths were studied, and the numerical results coincided with the experimental data. The mean offsets of sway motions also present an overall agreement with the results measured in the experiments. The flexibility of this combination of methods is attractive. Different geometrical bottom, oblique waves, and hydroelasticity of the floating body can be suggested as a topic of further research based on the computational model.

Data Availability

The experimental data used to support the findings of this study are available from the corresponding author upon request.

Conflicts of Interest

The authors declare that they have no conflicts of interest.

Acknowledgments

The corresponding author would like to thank Prof. Bernard Molin in Ecole Centrale Marseille, Sun Yat-sen University, for providing the experimental results.

References

[1] F. Stern, J. Yang, Z. Wang et al., "Computational ship hydrodynamics: nowadays and way forward," *International Shipbuilding Progress*, vol. 60, 2013.

[2] D. P. Rijnsdorp and M. Zijlema, "Simulating waves and their interactions with a restrained ship using a non-hydrostatic wave-flow model," *Coastal Engineering*, vol. 114, pp. 119–136, 2016.

[3] B. Bouscasse, A. Colagrossi, S. Marrone, and M. Antuono, "Nonlinear water wave interaction with floating bodies in SPH," *Journal of Fluids and Structures*, vol. 42, pp. 112–129, 2013.

[4] B. Ren, M. He, P. Dong, and H. Wen, "Nonlinear simulations of wave-induced motions of a freely floating body using wcsph method," *Applied Ocean Research*, vol. 50, pp. 1–12, 2015.

[5] K. A. Belibassakis, "A boundary element method for the hydrodynamic analysis of floating bodies in variable bathymetry regions," *Engineering Analysis with Boundary Elements*, vol. 32, no. 10, pp. 796–810, 2008.

[6] J. You and O. M. Faltinsen, "A numerical investigation of second-order difference-frequency forces and motions of a moored ship in shallow water," *Journal of Ocean Engineering and Marine Energy*, vol. 1, no. 2, pp. 157–179, 2015.

[7] L. Xiong, H. Lu, J. Yang, and W. Zhao, "Motion responses of a moored barge in shallow water," *Ocean Engineering*, vol. 97, pp. 207–217, 2015.

[8] S. Yan and Q. Ma, "Numerical simulation of fully nonlinear interaction between steep waves and 2d floating bodies using the qale-fem method," *Journal of Computational Physics*, vol. 221, no. 2, pp. 666–692, 2007.

[9] Q. W. Ma and S. Yan, "Qale-fem for numerical modelling of nonlinear interaction between 3d moored floating bodies and steep waves," *International Journal for Numerical Methods in Engineering*, vol. 78, no. 6, pp. 713–756, 2009.

[10] H. B. Bingham, "A hybrid boussinesq-panel method for predicting the motion of a moored ship," *Coastal Engineering*, vol. 40, no. 1, pp. 21–38, 2000.

[11] J. A. Pinkster and P. Naaijen, "Predicting the effect of passing ships," in *Proceedings of the 18th Int. Workshop on Water Waves and Floating Bodies*, Le Croisic, France, 2003.

[12] W. van der Molen and I. Wenneker, "Time-domain calculation of moored ship motions in nonlinear waves," *Coastal Engineering*, vol. 55, no. 5, pp. 409–422, 2008.

[13] J. P. H. Dobrochinski, "A Combination of Swash and Harberth to Compute Wave Forces on Moored Ships," Delft University of Technology, Delft, Netherlands, Civil Engineering and Geosciences, 2014.

[14] H. B. Bingham, P. A. Madsen, and D. R. Fuhrman, "Velocity potential formulations of highly accurate Boussinesq-type models," *Coastal Engineering*, vol. 56, no. 4, pp. 467–478, 2009.

[15] V. E. Zakharov, "Stability of periodic waves of finite amplitude on the free surface of a deep fluid," *Journal of Applied Mechanics and Technical Physics*, vol. 9, pp. 190–194, 1968.

[16] E. Jamois, *Interaction houle-structure en zone côtière*, PhD thesis, Université de la Méditerranée, Marseille, France, 2005.

[17] A. Quarteroni, R. Sacoo, and F. Saleri, *Numerical Mathematics*, Springer-Verlag, New York, NY, USA, 2000.

[18] Y. Saad and M. H. Schultz, "GMRES: a generalized minimal residual algorithm for solving nonsymmetric linear systems," *SIAM Journal on Scientific and Statistical Computing*, vol. 7, no. 3, pp. 856–869, 1986.

[19] Y. Liu, B. Molin, O. Kimmoun, F. Remy, and M.-C. Rouault, "Experimental and numerical study of the effect of variable bathymetry on the slow-drift wave response of floating bodies," *Applied Ocean Research*, vol. 33, no. 3, pp. 199–207, 2011.

[20] B. Molin, "Second-order hydrodynamics applied to moored structures," *Ship Technology Research*, vol. 41, pp. 59–84, 1994.

[21] H. Maruo, "The drift of a body floating in waves," *Journal of Ship Research*, vol. 4, pp. 1–10, 1960.

[22] J. N. Newman, "The drift force and moment on ships in waves," *Journal of Ship Research*, vol. 11, no. 01, pp. 51–60, 1967.

[23] J. A. Pinkster and O. G. Van Oortmerssen, "Computation of the first- and second-order wave forces on oscillating bodies in regular waves," in *Proceedings of the 2nd Int. Conf Numerical Ship Hydrodynamics*, pp. 136–156, California, USA, 1977.

[24] Y. Liu, *Effect Of Variable Bathymetry on the Linear and Slow-Drift Wave Responses of Floating Bodies*, PhD Thesis, Ecole Centrale Marseille, Marseille, France, 2010.

[25] W. Cummins, "The impulse response function and ship motions," *Schiffstechnik*, vol. 9, pp. 101–109, 1962.